Hindawi
International Journal of Aerospace Engineering
Volume 2022, Article ID 4045778, 10 pages
https://doi.org/10.1155/2022/4045778

Research Article

A Study on Hover Performance of Ducted Fans for an Unmanned VTOL Aircraft

Young Jae Choi, Seong-Yong Wie, and Sanghyun Chae

Aeronautics Technology Research Division, Korea Aerospace Research Institute, Daejeon 34133, Republic of Korea

Correspondence should be addressed to Seong-Yong Wie; wie@kari.re.kr

Received 21 April 2022; Accepted 10 July 2022; Published 25 July 2022

Academic Editor: Enrico Cestino

In this study, ground tests and numerical analysis were performed to verify the hover performance of the second ducted fan model designed by this research team. Shape of the duct inner surface was asymmetric in longitudinal direction, and considering various aspects such as test site or costs for test operation, a 40% scaled-down model of the ducted fan was adopted for this study. Both the results of the tests and the analysis were found to be coherent, and it was verified that the ducted fan was verified to be well designed to achieve the targeted performance. Furthermore, the performance of this ducted fan was compared with that of the symmetric one to determine the effects of the difference in the duct shape on the performance. It was observed that the symmetric ducted fan performs better in hovering flight, although the asymmetric ducted fan was sufficiently satisfied with the design intention.

1. Introduction

A ducted fan type is known to have advantages over the open rotor type in terms of thrust, noise, and safety [1]. Research on the ducted fan has been actively implemented from the early 2000s until recently, and the studies were mainly focused on a single ducted fan for a small UAV (unmanned aerial vehicle) that requires VTOL (vertical take-off and landing) ability in the 2000s [1–3]. After the 2010s, as VTOL vehicles of various concepts including small UAVs were introduced, various forms of ducted fans appeared naturally such as fan-in-wing [4–6], multiduct [7], and coaxial [8, 9] types. In addition, studies have been conducted on the performance of ducted fans in various ways. Ohanian et al. studied how to represent the ducted fan aerodynamics with nondimensional coefficients [10]. Liu et al. [11] and Bontempo and Manna [12] studied the effects of the duct geometry on the performance. Furthermore, there were studies on the effects of artificial flows on the ducted fan. Sheng and Zhai [13] conducted numerical investigations of the ducted fan with active flow control devices that perform suction and injection of flows near the duct inner surface of the duct, and Chen et al. [14] examined the ducted fan with tip jets numerically.

This research team of KARI has also been researching the performance of ducted fans [15–17] and recently designed the second ducted fan model for an unmanned VTOL aircraft currently being developed. The duct shape of the second model was designed asymmetrically in the longitudinal direction with the expectation of better performance in forward flight than a symmetric ducted fan. However, the present study is focused only on the hover performance, and the forward flight performance will be investigated in the next study with the wind-tunnel tests. The first purpose of the present study is to verify whether the second model achieves the intended hover performance of the design, and the second purpose is to determine how different the hover performance of the second model from that of the symmetric one. The hover performance of the symmetric one was already obtained through the previous studies

(a) Symmetric ducted fan (b) Asymmetric ducted fan

Figure 1: Cross-section in longitudinal direction of both designed ducted fans.

Figure 2: The 40% scaled-down ducted fan model and the configuration of the test stand.

[16], and the symmetric ducted fan was the first model designed by this research team. In the present study, the ground tests and the CFD (computational fluid dynamics) analysis were conducted by using a scaled-down model as was done for the first model to accomplish both purposes, and the hover performance of both ducted fans was compared with each other.

2. Ducted Fan System

2.1. Configuration of Ducted Fan Model. The second ducted fan used in this study was designed by this research team to satisfy specific performance such as the duct thrust ratio and hovering efficiency. Only the inner surface shape was designed asymmetrically in the longitudinal direction, and the fan blades were maintained the same as the first model. It was composed of six blades and a single duct, and the clearance between the blade and the duct in the rotational plane was designed to be 1% of the inner radius of the duct. The inner radius of the duct was designed to be 1 m. The cross-section of the blade was designed as a "NACA23012" airfoil, and the distribution of the twist angle was nonlinear [16]. Figure 1 represents the cross-section in the longitudinal direction between the first model, which is a symmetrical ducted fan, and the second model, which is an asymmetric ducted fan. The terms of the first ducted fan model and the second ducted fan model used in this paper were to be unified as "symmetric ducted fan" and "asymmetric ducted fan," respectively. In this study, a 40% scaled-down model was used taking into account various aspects such as test site and costs of manufacturing or operating the test model.

2.2. Hover Performance of a Ducted Fan. The hover performance of a ducted fan is generally examined by thrust, power, duct thrust ratio, and figure of merit [18]. In this paper, thrust and power performance were represented as thrust coefficient (C_T) and power coefficient (C_P), defined as Equations (1) and (2), respectively, where "ρ" is the air density, "A" is the disk area, and "V_{Tip}" is the speed of the blade tip. In addition, "T" represents the total thrust of the ducted fan, and "P" represents the fan power.

$$C_T = \frac{T}{\rho A V_{Tip}^2}, \tag{1}$$

$$C_P = \frac{P}{\rho A V_{Tip}^3}. \tag{2}$$

The duct thrust ratio was calculated by the ratio of the difference between the total thrust and the fan thrust to the total thrust, as shown in Equation (3), where "T_F" represents the fan thrust of the ducted fan.

$$\text{Duct Thrust Ratio} = \frac{T - T_F}{T}. \tag{3}$$

The figure of merit is a dimensionless number defined as the ratio of the ideal fan power to the measured fan power as expressed in

$$\text{Figure of Merit} = \frac{P_{\text{ideal}}}{P}. \tag{4}$$

"$P_{F,\text{ideal}}$" in Equation (4) is computed by Equation (5), and "a_ω" in Equation (5) is a parameter related to the duct wake area [18].

$$P_{\text{ideal}} = \frac{T^{3/2}}{\sqrt{4 a_\omega \rho A}}. \tag{5}$$

In this study, the collective pitch angle that means the pitch angle at 75% of the blade radius was considered in the range of 20 to 36 degrees. The rotation speed was determined to be 4000 RPM to maintain the Mach number similarity with the full-scale model.

3. Experimental and Numerical Methods

3.1. Ground Tests. The ducted fan model for ground tests was installed at a position where the height of the rotating

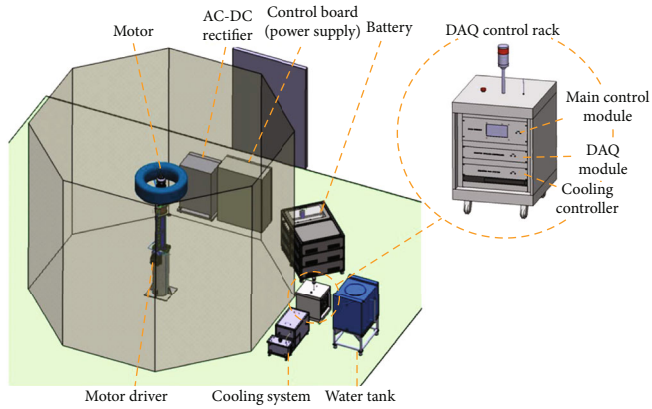

Figure 3: Layout of the facilities to operate the ducted fan performance tests.

surface from the ground was about 4.2 times the inner diameter of the duct, and a column-shaped support structure was built under the ducted fan as shown in Figure 2. The rotation of the fan was driven by using the "EMRAX 228" motor that can drive up to 109 kW of power [19], and test devices essential for driving the motor such as a motor driver, power supply, and cooling system were also prepared. In addition, a safety fence was also constructed and the test devices were arranged as shown in Figure 3. To acquire the thrust and torque data from performing the tests, two loadcells were mounted between the ducted fan and the support structure. The "Loadcell 1" was used to measure the thrust and torque generated by the rotating fan, and the "Loadcell 2" was used to measure the total thrust of the ducted fan in the ground tests. The data of each condition were acquired for about five seconds at a sampling rate of 10 kHz, and the averaged value of the data was used.

Ground tests were carried out in the RPM-sweep method, which fixed the pitch angle and increased the RPM to the target value of 4000 RPM, since the pitch angle was manually adjusted. The pitch angle conditions performed in the test were 20, 24, 28, 30, 32, and 36 degrees. The speed of fan rotation was increased in units of 1000 or 500 RPM up to 4000 RPM, and data at each RPM was also measured. In order to increase the reliability of the acquired data, the test was conducted three times for each condition.

3.2. Repeatability of Data Acquisition from the Test Facilities. Before conducting the main tests, it is necessary to verify the repeatability of the data acquisition from the test equipment. Therefore, one of the collective pitch angle conditions to be performed in the tests was selected for verification of the repeatability, and it was the pitch of 30 degrees. The test was carried out three times under the same conditions and they were labeled "Run1," "Run2," and "Run3" in order of test execution. The thrust and torque were measured in each test, and torque data were converted into the power performance. Figure 4 shows the total thrust and fan power of all the measured RPMs as dimensional and nondimensional performance. It was confirmed that the performance data obtained in the three tests were measured equally at each RPM, and it was also found that the similarity was well maintained in all the measured RPMs through the performance expressed as a dimensionless coefficient. As a result, it was verified that the test device currently prepared has repeatability in data acquisition. In Figure 4, the interval between each tick of (a) thrust, (b) power, (c) thrust coefficient, and (d) power coefficient is 1000 N, 20 kW, 0.1, and 0.01, respectively.

3.3. Computational Fluid Dynamics. CFD analysis was performed with the STAR-CCM+ (ver.15.02), a commercial software that can solve the Navier-Stokes equations numerically, and the reliability of the results for the ducted fan was already validated through previous studies [16]. To calculate the fan rotations in time, the sliding mesh technique was performed, and the time step was set as the time for the fan to rotate 3 degrees. In addition, a dual time stepping technique was adopted, and the number of iterative calculations at each time step was set to 20. The convective terms in the N-S equations were discretized using Roe's flux difference splitting scheme, and the diffusive terms were discretized by the central difference method [20]. Turbulent viscosity was computed by the Spalart-Allmaras model.

The computation conditions were adopted the same as the test conditions. However, the rotational speed of the fan was only prepared at 4000 RPM in consideration of computational resources and time. The computational domain was composed of the ducted fan model with the support structure and the ground, as shown in Figure 5, and the far boundary condition of the freestream and the pressure outlet was located at a distance of 20 times the inner diameter of the duct of the model. Atmospheric pressure and temperature were set as 104300 Pa and 26°C, respectively, since they were averaged atmospheric conditions when the tests were conducted.

3.4. Computational Grids. To decide a computational grid, a grid dependency test was performed. Three different grids composed of about 8 million/15 million/20 million polyhedral cells were generated for the grid dependence test, and they were named as "Coarse," "Medium," and "Fine,"

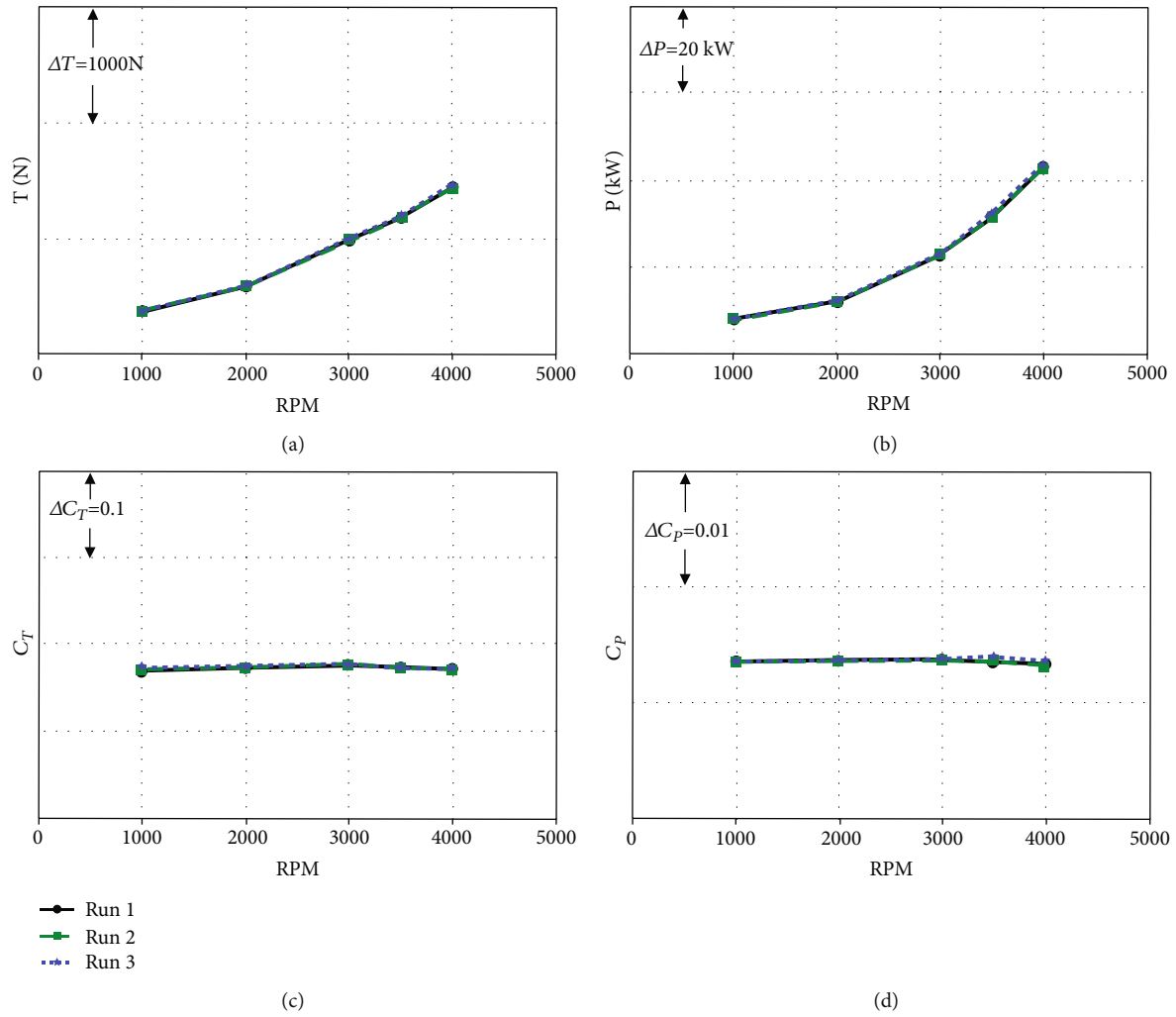

Figure 4: Results of repeatability tests to verify the DAQ system of the test facilities. The results were expressed by the (a) thrust, (b) power, (c) thrust coefficient, and (d) power coefficient with respect to RPMs.

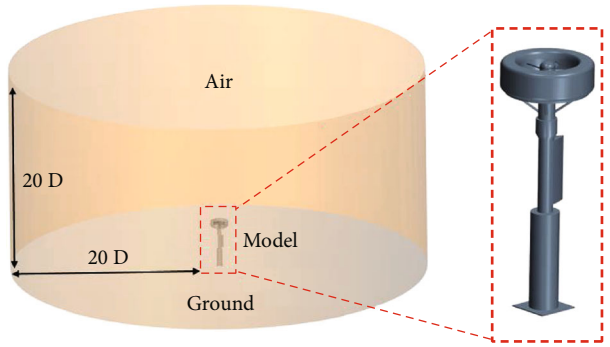

Figure 5: Computational domain and the configuration of the CFD model.

respectively, as shown in Figure 6. The computational conditions for the grid dependency test were selected as one of the conditions for CFD analysis: a collective pitch angle of 30 degrees at 4000 RPM.

The results were represented by hover performance as shown in Figure 7, and the performance data were computed by averaging the performance of the last three revolutions. It was confirmed that the "Coarse" results differed more than 3% from the "Fine" results, and the "Medium" results differed less than 1% from the "Fine" results. As a result, the computational grid was determined as the "Medium" meshes in consideration of solution accuracy, computational resources, and time, and a cross-sectional view of the computational grid was depicted in Figure 8. The maximum cell size on the blade surface was limited to 11% of the blade chord length, and the cell size near the ground was generated to be around 71% of the chord length. Reichardt's blended function was used to generate the meshes near the wall [21], and the maximum size of the initial prism layer ($y+$) was composed of around 1.8.

4. Results and Discussion

4.1. Hover Performance of the Asymmetric Ducted Fan. The hovering performance of the asymmetric ducted fan through

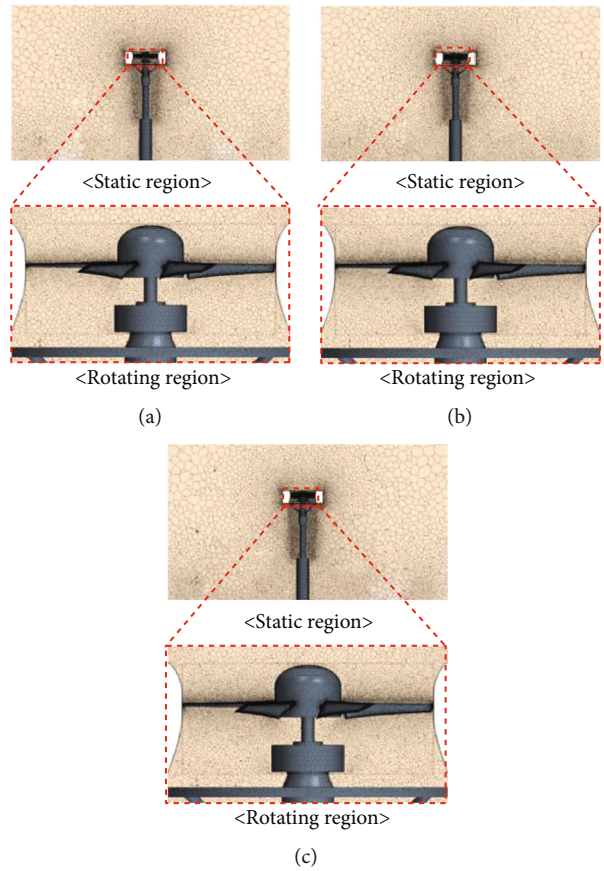

Figure 6: Comparison of the three different grids using in the grid dependency tests. (a) Coarse. (b) Medium. (c) Fine.

the tests and the CFD analysis was compared in Figure 9. On the graphs, the circular marker indicates the test results, and the solid line indicates the CFD results. The thrust performance in Figure 9(a) was expressed by the thrust coefficient normalized by the thrust coefficient of the targeted thrust. First, it was shown that the thrust increases linearly as the pitch angle increases in both the tests and the CFD. Furthermore, it was confirmed that the target thrust was achieved at a pitch angle of about 31 degrees or more. However, it was found that the CFD results of the thrust were predicted to be slightly higher than the test results. It seemed that there was a little difference on the actual pitch angles comparing to the computation because the pitch angles were manually adjusted in the test. The reason for this judgment was that the power curves along the thrust were almost matched in both the tests and the CFD as shown in Figure 9(b), although the absolute value of the thrust in the tests differs from the CFD results at same pitch angles. It was observed that the power and the thrust were related to a function of quadratic or higher polynomials, and it was indicated that the tests and the CFD analysis were performed well from the power curve results. The interval between each tick of the power coefficient is 0.01 in the graph. Furthermore, it was identified that the duct thrust ratio was about 0.25 higher than the target performance, and it was found that the duct thrust ratio was maintained above a certain level regardless of the increase or decrease in thrust, as shown in Figure 9(c). The interval between each tick of the duct thrust ratio is 0.25. Finally, the results of the figure of merit, which means the efficiency of hovering flight, are presented in Figure 9(d). The interval between each tick of the figure of merit in the graph is 0.25. It was obtained that the figure of merit was achieving the target performance under all the conditions of the tests and the CFD, and it was also indicated that the figure of merit above a certain level was maintained regardless of the increase or decrease of the thrust, similar to the duct thrust ratio. Therefore, it was verified that the asymmetric ducted fan was designed well to perform the required performance.

4.2. Effects of the Difference in Duct Shape on Hover Performance. The hovering performance of the asymmetric ducted fan was compared with that of the symmetric one already obtained through the preceding study [16] as shown in Figure 10. In the graphs, the green square and the blue dotted line represent the performance of the symmetric ducted fan [16], and the black circle and the red solid line represent the performance of the asymmetric ducted fan. In addition, both square and circle markers mean the test results, and both dotted and solid lines mean the CFD results. It was found that the thrust of the symmetric ducted fan was about 3% higher than that of the asymmetric at the

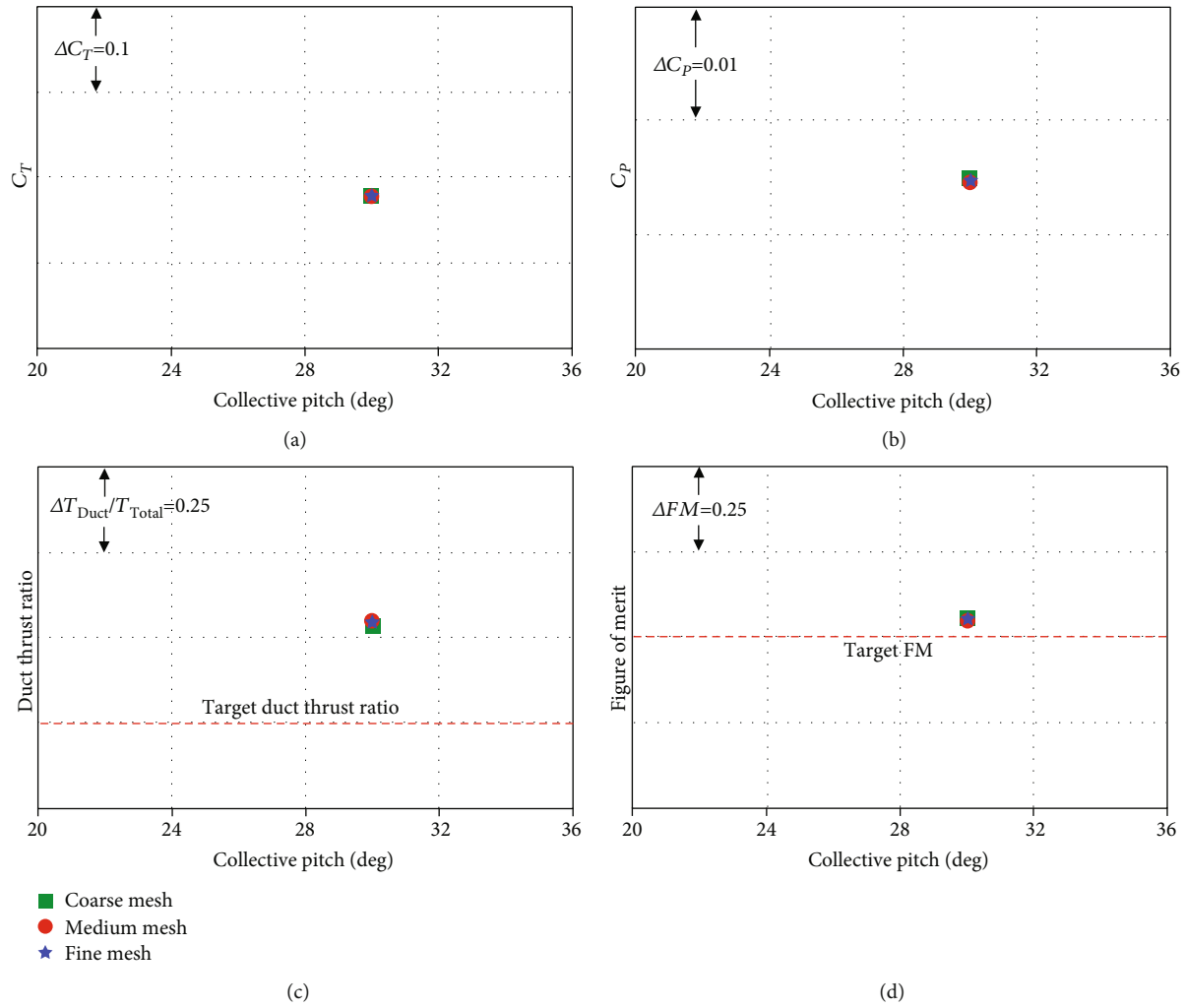

Figure 7: Results of the grid dependency tests. The results were represented by the hover performance: (a) thrust coefficient, (b) power coefficient, (c) duct thrust ratio, and (d) figure of merit.

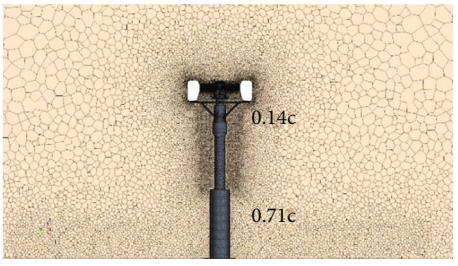

Figure 8: Grid topology of the "Medium" meshes in the transverse plane.

same pitch angle, meaning that the asymmetric ducted fan requires more power than the symmetric one to produce the same thrust. It was observed that these characteristics also appeared consistently in the duct thrust ratio and the figure of merit.

In order to examine the cause of the difference in the performance in more detail, the CFD results were further investigated. The results of the pitch of the 32-degree among the various conditions were selected, and the flows around both ducted fans were visualized by vorticity, velocity, and pressure contours to compare the aerodynamic characteristics as shown in Figures 11 and 12. The left side of the figures represents the results of the symmetric ducted fan, and the right side represents the results of the asymmetric ducted fan. It was shown that the flow passing through the asymmetric duct was deflected to the rear of the duct unlike the symmetric ducted fan. Besides, it was observed that the flow passing through the asymmetric duct was separated from the inner surface on the duct front while the flow passing through the symmetric duct was not separated. These phenomena were expected to be explained with the pressure distributions around the asymmetric ducted fan as shown in Figure 12. In particular, a relatively higher pressure region was developed at the lower end of the asymmetric duct front than at the lower end of the duct rear due to the difference in the shape of the inner surface in longitudinal direction. In addition, it was verified that the pressure imbalance occurred on the asymmetric duct makes the flow biased

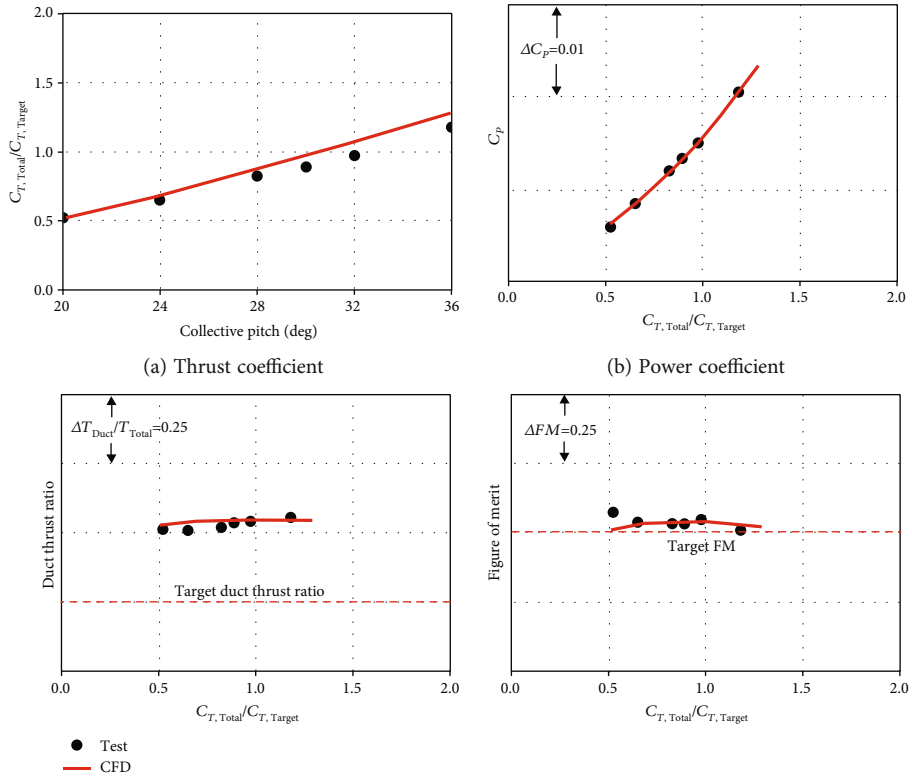

(a) Thrust coefficient

(b) Power coefficient

(c) Duct thrust ratio

(d) Figure of merit

Figure 9: Hover performance of the asymmetric ducted fan.

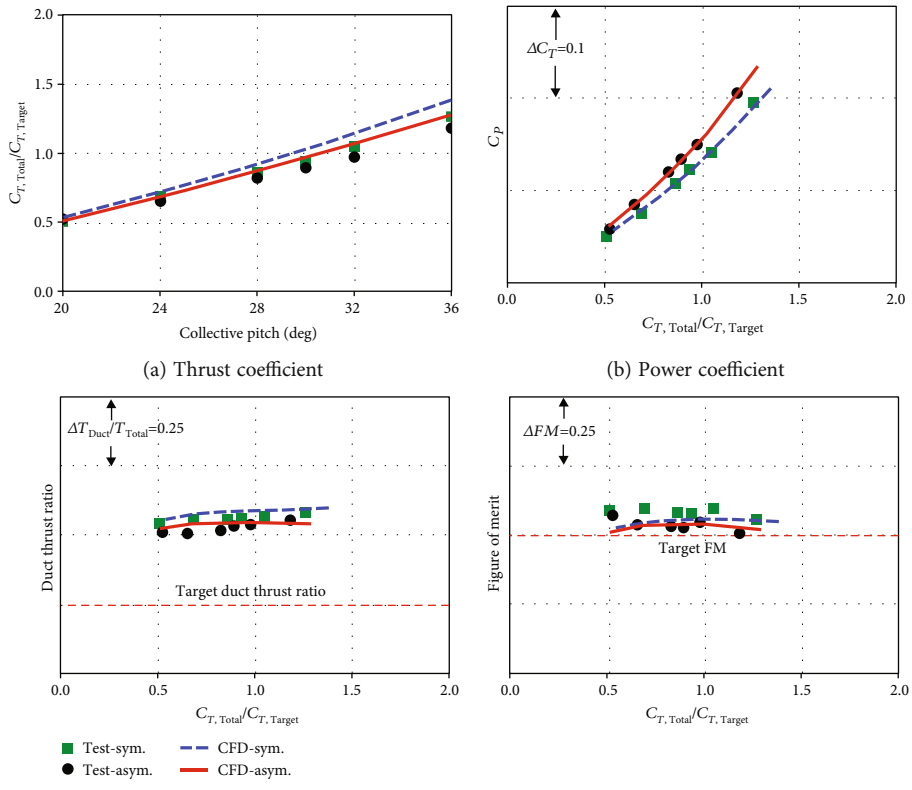

(a) Thrust coefficient

(b) Power coefficient

(c) Duct thrust ratio

(d) Figure of merit

Figure 10: Hover performance of both symmetric and asymmetric ducted fans.

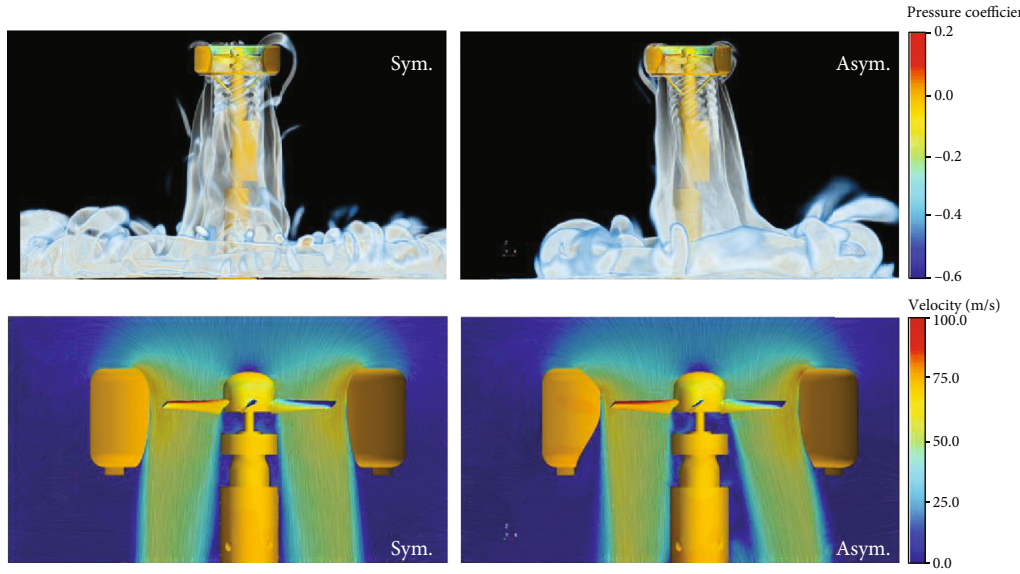

Figure 11: Vorticity and velocity distributions around both symmetric and asymmetric ducted fan.

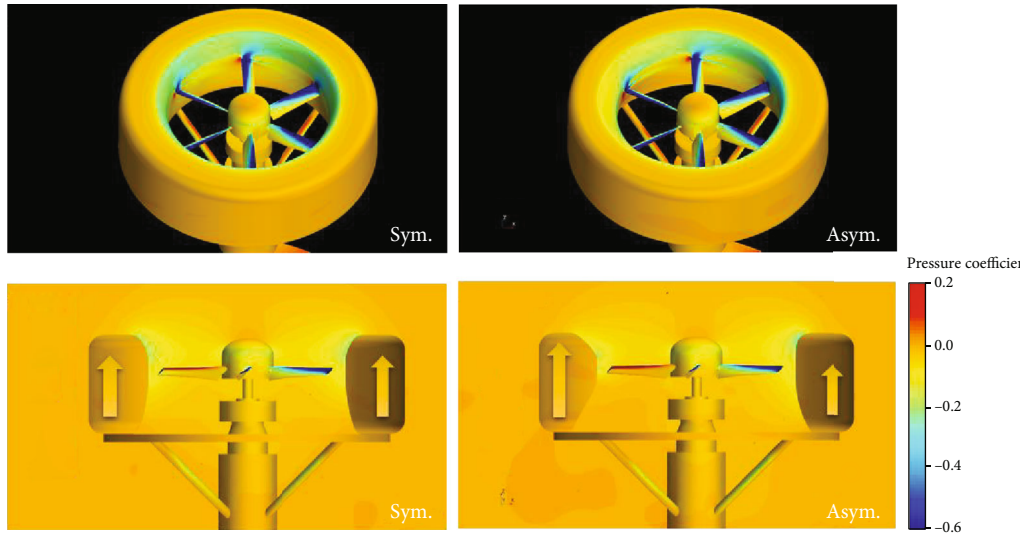

Figure 12: Pressure distributions around both symmetric and asymmetric ducted fan.

towards the rear of the duct. Furthermore, it was perceived that the pressure imbalance around the asymmetric duct makes the thrust distributions be weighted on the duct front as depicted in Figure 12, and it was expected that these unbalanced thrust distributions produce the pitching moment on the duct simultaneously.

In this regard, the pitching moment data was also extracted from the CFD results and compared with each other as represented in Figure 13. The pitching moment in this paper was expressed by the quantity normalized by the reference value, which is the targeted thrust multiplied by the radius of the fan blade. In the graph, the dotted line represents the symmetric ducted fan, and the solid line represents the asymmetric ducted fan. It was observed that the pitching moment actually occurred on the asymmetric ducted fan as the expectation, although the pitching moment was relatively small value in a positive direction. On the contrary, the pitching moment of the symmetric ducted fan was maintained almost zero. Moreover, the pitching moment of the asymmetric ducted fan increases as the pitch angle increases. Therefore, it was determined that the symmetric ducted fan has advantages in hovering flight and the stability compared to the asymmetric one.

5. Conclusions

In this study, in order to verify the hover performance of the asymmetric ducted fan, which is the second model designed by this research team of KARI, both the ground tests and the CFD analysis were conducted with the 40% scaled-down model. It was observed that both the tests and the CFD were coherent, and it was verified that the ducted fan was well designed to achieve the target performance. It was also found that hover performance of the full-scale ducted fan

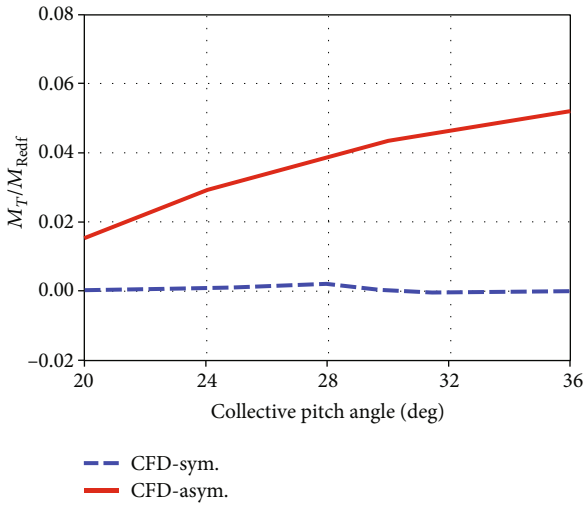

Figure 13: Pitching moment of both symmetric and asymmetric ducted fan.

could be predicted indirectly through the nondimensional performance of the scaled-down model because of its similarity. In addition, the performance of the asymmetric ducted fan was compared with the performance of the first designed ducted fan, the symmetric ducted fan, obtained from preceding studies [16] to identify the effects of difference in the duct shape on the performance. It was found that the symmetric ducted fan performs better in hovering flight although the asymmetric one was designed to achieve the targeted performance. Furthermore, the CFD results were visualized to compare the difference in flows around both ducted fans. Unbalanced thrust distributions were developed on the asymmetric duct surface due to the characteristics of its shape, and these phenomena would have an adverse effect on stability. Consequently, these results implied that the symmetric ducted fan is better choice for hovering flight than the asymmetric one, and these results will be used as important data to determine the final ducted fan design to be applied to the unmanned VTOL aircraft currently under development.

Data Availability

The performance data used to support the findings of this study have not been made available because the agency that supported this study requested confidentiality.

Conflicts of Interest

The authors declare that there is no conflict of interest regarding the publication of this paper.

Acknowledgments

This work was supported by a grant (UC170032JD) from the Agency for Defense Development (ADD), Korea.

References

[1] J. L. Pereira, "Hover and wind-tunnel testing of shrouded rotors for improved micro air vehicle design," *Ph.D. dissertation*, University of Maryland, 2008.

[2] A. I. Abrego and R. W. Bulaga, "Performance study of a ducted fan system," in *Proc. AHS specialists meeting on aerodynamics, acoustics, and test and evaluation*, San Francisco, CA, 2002.

[3] W. E. Graf, "Effects of duct lip shaping and various control devices on the hover and forward flight performance of ducted fan UAVs," *M.S. thesis*, Virginia Polytechnic Institute and State University, 2005.

[4] J. H. Moon, H. G. Lee, and J. S. Cho, "Study for fan-in-wing UAV flow characteristics," *The KSFM Journal of fluid machinery*, vol. 22, no. 6, pp. 22–29, 2019.

[5] N. Y. Roh, S. J. Oh, and D. H. Park, "Aerodynamic characteristics of helicopter with ducted fan tail rotor in hover under low-speed crosswind," *International journal of aerospace engineering*, vol. 2020, Article ID 7059209, 14 pages, 2020.

[6] B. Hoeveler, A. Bauknecht, C. C. Wolf, and F. Janser, "Wind-tunnel study of a wing-embedded lifting fan remaining open in cruise flight," *Journal of Aircraft*, vol. 57, no. 4, pp. 558–568, 2020.

[7] M. H. Ryu, L. S. Cho, and J. S. Cho, "Aerodynamic analysis of the ducted fan for a VTOL UAV in crosswinds," *Transactions of the Japan Society for Aeronautical and Space Sciences*, vol. 59, no. 2, pp. 47–55, 2016.

[8] Y. Jian, H. Li, and H. Jia, "Aerodynamics optimization of a ducted coaxial rotor in forward flight using orthogonal test design," *Shock and vibration*, vol. 2018, Article ID 2670439, 9 pages, 2018.

[9] S. Deng, S. Wang, and Z. Zhang, "Aerodynamic performance assessment of a ducted fan UAV for VTOL applications," *Aerospace Science and Technology*, vol. 103, p. 105895, 2020.

[10] O. J. Ohanian, P. A. Gelhausen, and D. J. Inman, "Nondimensional modeling of ducted-fan aerodynamics," *Journal of Aircraft*, vol. 49, no. 1, pp. 126–140, 2012.

[11] P. Liu, N. Shiomi, Y. Kinoue, Y. Z. Jin, and T. Setoguchi, "Effect of inlet geometry on fan performance and flow field in a half-ducted propeller fan," *International Journal of Rotating Machinery*, vol. 2012, Article ID 463585, 9 pages, 2012.

[12] R. Bontempo and M. Manna, "Effects of duct cross section camber and thickness on the performance of ducted propulsion systems for aeronautical applications," *International Journal of Aerospace Engineering*, vol. 2016, Article ID 8913901, 9 pages, 2016.

[13] C. Sheng and Q. Zhai, "Numerical investigations of fan-in-wing aerodynamic performance with active flow control," *Journal of Aircraft*, vol. 54, no. 6, pp. 2317–2329, 2017.

[14] J. Chen, L. Li, G. Huang, and X. Xiang, "Numerical investigations of ducted fan aerodynamic performance with tip-jet," *Aerospace Science and Technology*, vol. 78, pp. 510–521, 2018.

[15] H. J. Kang, "Aerodynamic analysis in forward flight for the ducted fan system of a compound rotorcraft," in *Proceeding of the Korean society for aeronautical and space science spring conference*, pp. 236-237, 2019.

[16] Y. J. Choi, S. W. Wie, B. I. Yoon, and D. H. Kim, "A study on hovering performance of ducted fan system through ground tests and CFD simulations," *Journal of the Korean society for aeronautical and space science*, vol. 49, no. 5, pp. 399–405, 2021.

[17] B. I. Yoon, Y. J. Choi, S. W. Wie, and S. H. Chae', "Test for measuring flow velocity downstream of ducted fan system," in *Proceeding of the Korean society for aeronautical and space science fall conference*, pp. 1038-1039, 2021.

[18] J. G. Leishman, *Principle of Helicopter Aerodynamics*, Cambridge University Press, 2nd edition, 2006.

[19] https://emrax.com/e-motors/emrax-228.

[20] J. Blazek, *Computational Fluid Dynamics: Principles and Applications*, Elsevier Science Ltd., 2001.

[21] H. Reichardt, "Vollständige darstellung der turbulenten geschwindigkeitsverteilung in glatten leitungen," *Journal of Applied Mathematics and Mechanics*, vol. 31, no. 7, pp. 208–219, 1951.